JOURNAL OF MATERIALS SCIENCE: MATERIALS IN MEDICINE 1 (1990) 81–89

A water transport model for the creep response of the intervertebral disc

J. J. CASSIDY*, M. S. SILVERSTEIN‡, A. HILTNER, E. BAER
Department of Macromolecular Science and Center for Applied Polymer Research, Case Western Reserve University, Cleveland, Ohio 44106, USA

Time-dependence in the mechanical response of the intervertebral disc has previously been shown to arise from the transport of water out of the disc. A creep model has been devised which describes the water transport in terms of the disc structure. This model assumes that the flow of water is the result of a pressure gradient across the cartilage end-plates, caused by an externally applied stress. The fluid transport properties of the cartilage determine the flow rate. Several cases are studied; those that best fit the experimental results use either a strain-dependent or a time- and strain-dependent pressure gradient. The permeability of the disc system is in the range (0.20 to 0.85) $\times 10^{-17} m^4 N^{-1} sec^{-1}$ and depends on the stress level. These values are lower than those reported in the literature for articular cartilage, but this can be explained in part by the differences in water content of the cartilage types. Permeability is found to decrease with applied stress, and both the strain- and time-dependence parameters increase in magnitude with stress. It can be shown that the analytical models of the creep response of the disc are analogous to three- and four-parameter viscoelastic models that employ springs and dashpots.

1. Introduction

Viscoelastic models employing springs and dashpots are frequently used to describe time-dependent relaxation processes in biological materials. However, the elements of these models are not directly related to the structure of the material. In order to understand the relationship between the macroscopically measured mechanical properties and the hierarchical structure of the biological system, it is necessary to develop physiologically meaningful models.

It was shown previously that compressive stress relaxation of the intervertebral disc occurs by loss of water from the disc structure [1]. This mechanism differs fundamentally from the molecular reorganization normally associated with the relaxation behaviour of materials, but is similar to that of articular cartilage, which also relaxes by means of water transport through cartilaginous material [2]. Numerous studies have characterized the compressive creep behaviour of articular cartilage in terms of a transport coefficient, usually the permeability [3–5]. The disc and articular cartilage systems are not completely analogous, however. Indentation testing of cartilage results in compaction of the cartilage, which decreases in thickness as water is squeezed out at the free surface [6], much as stepping on wet sand forces water to the surface. In comparison, the disc is tested in compression as a system; the cartilage end-plates are considered to be essentially rigid, porous structures that do not deform, while the compressed disc acts as a pump to force water through the pores of the cartilage into the cancellous bone of the vertebral bodies. Consequently, in order to describe the time-dependent response of the disc, it is necessary to formulate new models that are derived specifically from the structure of the intervertebral disc system.

2. Creep models

2.1 Anatomical basis

The intervertebral disc is modelled as a system consisting of the disc together with the cartilage end-plates attached to the vertebral bodies [7]. The disc is deformable and, when a compressive load is applied, the annulus fibrosus bulges outwards. A restoring force resisting this bulging is provided by the collagen fibres of the lamellae that comprise the annulus. These fibres are loaded in tension when the disc is compressed [1]. This compression creates a pressure within the disc, which is the driving force for water to flow through the cartilage end-plates and into the vertebral bodies. From there, the water is transported by the circulatory system away from the vertebrae. The strain in the lamellae of the annulus is relieved by the decrease in volume of the disc as water flows out. This model is shown schematically in Fig. 1. In the following analysis the cartilage end-plates and vertebral bone are assumed to be incompressible. It is also assumed that the permeability of the cartilage controls the rate at which water is expressed from the compressed disc.

* *Present address*: Richards Medical Co., Memphis, Tennessee 38116, USA.
‡ *Present address*: Department of Materials Engineering, Technion, Haifa 32000, Israel.

0957–4530/90 $03.00 + .12

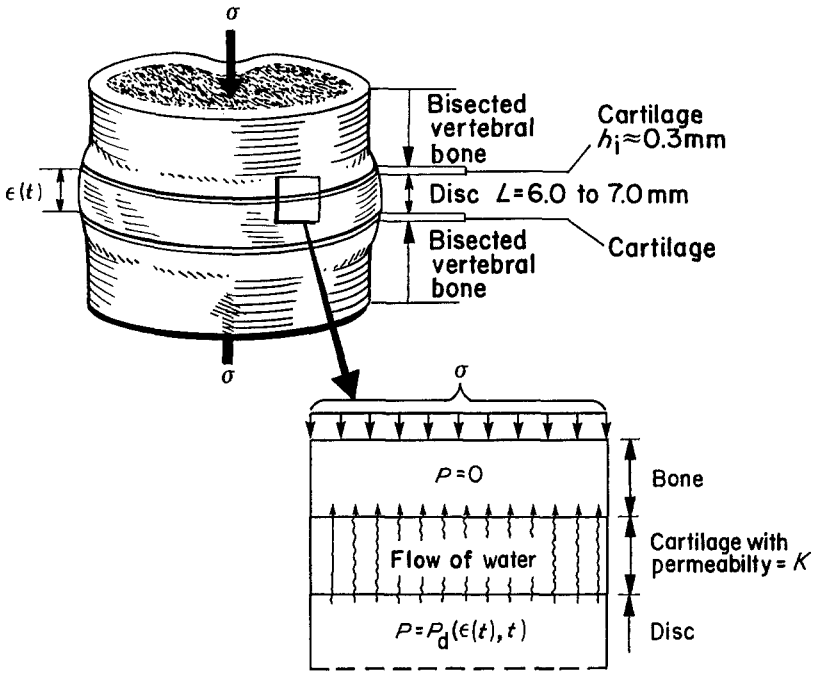

Figure 1 Creep model of the intervertebral disc.

2.2. Analytical model

It is assumed that compressive creep is due to the flow of water out of the disc as the result of the pressure gradient across the cartilage end-plates caused by an externally applied stress. The hydrostatic pressure within the disc, P_d, is not necessarily equal to the externally applied stress, σ_0, neither is is necessarily a constant. Both the strain- and the time-dependences of the pressure gradient across the cartilage are considered. Within the disc the hydrostatic pressure is assumed to be homogeneous.

The relationship between the volumetric flux and the pressure gradient is modelled by Darcy flow in a quasi-steady-state system. Laminar flow and a linear pressure gradient across the cartilage end-plates are assumed. The Darcy equation is applied to the total volume flux from the disc through two cartilage end-plates (above and below the disc) having a permeability coefficient K. The relationship between the hydrostatic pressure, P_d, and the strain, $\varepsilon(t)$, is given by

$$q = h_i \frac{d[\varepsilon(t) - \varepsilon_0]}{dt} = \frac{2K}{L} P_d \qquad (1)$$

where h_i is the height of the disc before testing (m), $\varepsilon(t)$ is the strain, q is the volume flux ($m^3 m^{-2} sec^{-1}$), t is the time (sec), ε_0 is the strain at $t = 0$, P_d is the pressure in the disc ($N m^{-2}$), L is the thickness of the barrier layer, in this case the cartilage (m) and K is the permeability constant ($m^4 N^{-1} sec^{-1}$).

Three cases are considered for the hydrostatic pressure in the disc.

Case I: Constant hydrostatic pressure.

Case II: Strain-dependent hydrostatic pressure.

Case III: Strain- and time-dependent hydrostatic pressure.

Case I. Constant pressure

In case I the hydrostatic pressure within the disc, P_d, is assumed to be constant for the duration of the creep experiment and equal to the difference between the applied stress, σ_0 ($N m^{-2}$), and the osmotic pressure in the disc, P_0 ($N m^{-2}$), as shown by

$$P_d = \sigma_0 - P_0 \qquad (2)$$

This expression for the hydrostatic pressure is substi-

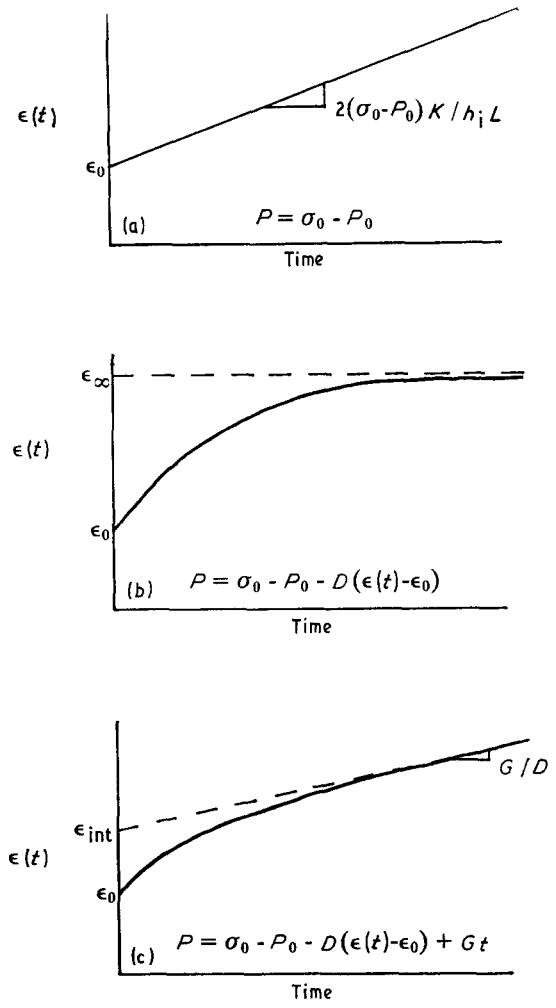

Figure 2 Three cases of the creep model. (a) Case I: constant pressure gradient; (b) case II: strain-dependent pressure gradient and (c) case III: time- and strain-dependent pressure gradient.

tuted into Equation 1 and, upon integration, gives a linear relationship between strain and time:

$$\varepsilon(t) = \varepsilon_0 + \frac{2(\sigma_0 - P_0)K}{h_i L} t \quad (3)$$

Equation 3 predicts a linear creep curve (Fig. 2a) and the permeability, K, can be calculated from the slope. Since the experimental creep data are not linear, it is necessary to consider cases where the hydrostatic pressure is not constant.

Case II. Strain-dependent pressure

Case II considers the increase in osmotic pressure as the amount of water in the disc decreases. This increase in osmotic pressure is assumed to be linear with strain, and

$$P_d = \sigma_0 - \{P_0 + D[\varepsilon(t) - \varepsilon_0]\} \quad (4)$$

gives the hydrostatic pressure within the disc where the system parameter D ($N\,m^{-2}$) represents the magnitude of the strain-dependence. Substitution of this relationship into Equation 1 and integration yields the strain as a function of exponential time:

$$\varepsilon(t) = \varepsilon_0 + \frac{\sigma_0 - P_0}{D}\left[1 - \exp\left(-\frac{2KDt}{h_i L}\right)\right] \quad (5)$$

According to this equation, the strain reaches an asymptotic value, ε_∞, as the exponential term becomes negligible at long times (Fig. 2b), and Equation 5 reduces to

$$D = \frac{\sigma_0 - P_0}{\varepsilon_\infty - \varepsilon_0} \quad (6)$$

The system parameter D can be calculated from Equation 6. Equation 6 is substituted into Equation 5 to yield

$$-\ln\frac{\varepsilon(t) - \varepsilon_\infty}{\varepsilon_0 - \varepsilon_\infty} = \frac{2KD}{h_i L} t \quad (7)$$

Using the value of D obtained from Equation 6, the permeability, K, is calculated from the slope of the plot of $-\ln\{[\varepsilon(t) - \varepsilon_\infty]/(\varepsilon_0 - \varepsilon_\infty)\}$ against t.

Case III. Time- and strain-dependent pressure

Although it will be seen that case II adequately describes the experimental observations, it does not take into consideration the probability that the retractile force exerted by the collagen fibres in the lamellae of the annulus fibrosis is time-dependent. The well-known viscoelastic character of collagen fibres [8] would introduce certain features into the creep curve that could not be confirmed in this study due to the limitations of the experiment. As indicated above, case II requires that the strain reaches an asymptotic value at long times. It is possible that the disc does not exhibit such behaviour. It is also possible that the disc may exhibit non-recoverable strain when unloaded, although this could not be determined from *in vitro* measurements on the open system. Both of these phenomena can be accommodated by adding a linear, time-dependent term to the hydrostatic pressure. This is illustrated in Equation 8, where the system parameter G ($N\,m^{-2}\,sec^{-1}$), represents the magnitude of the time-dependence:

$$P_d = \sigma_0 - \{P_0 + D[\varepsilon(t) - \varepsilon_0] - Gt\} \quad (8)$$

Substituting Equation 8 into Equation 1 and integrating yields

$$\varepsilon(t) = \varepsilon_0 + \left(\frac{\sigma_0 - P_0}{D} - \frac{h_i LG}{2KD^2}\right) \times \left[1 - \exp\left(-\frac{2KDt}{h_i L}\right)\right] + \frac{G}{D} t \quad (9)$$

which has both an exponential and a linear dependence of strain on time (Fig. 2c).

At long times the exponential term in Equation 9 is negligible and the relationship between strain and time is linear with a slope of G/D. The intercept of this linear region extrapolated to the strain axis, ε_{int}, is given by

$$\varepsilon_{int} = \varepsilon_0 + \frac{\sigma_0 - P_0}{D} - \frac{h_i LG}{2KD^2} \quad (10)$$

and is a function of the system parameters K, D and G. When Equation 10 is substituted into Equation 9, we obtain

$$-\ln\left(\frac{\varepsilon(t) - \varepsilon_{int} - (G/D)t}{\varepsilon_0 - \varepsilon_{int}}\right) = \frac{2KD}{h_i L} t \quad (11)$$

Using the value of G/D obtained from the slope of the linear, long-time region of the creep curve, a plot of the quantity on the left-hand side of Equation 11 against t should be linear with a slope equal to $2KD/h_i L$). Equations 10 and 11 can then be solved simultaneously to calculate the values of K and D.

3. Verification of the models

3.1. Experimental methods

Spinal segments were harvested from adult mongrel canines. Discs from two different animals were used in the tests. The discs selected were from levels T11–T12 to L6–L7. Spinal segments were divided into groups of three adjacent discs, with each disc in a group tested at a different stress level. Isolated disc specimens were prepared by cutting transversely through the vertebral bones above and below the disc. These cuts were made parallel to the disc. The posterior articulating facets and bony processes were removed. The resultant test specimens consisted of a disc with approximately 10 mm viable bone above and below. The area of the disc was determined by measuring the maximum and minimum diameters of the disc and applying the area formula for an ellipse. A correction factor was used to account for deviation of the disc from this idealized geometry [1]. Discs were enclosed in plastic to maintain 100% relative humidity. Discs were used fresh or kept refrigerated at 4° C until tested. All were tested within 72 h of removal. Before testing, specimens were equilibrated at room temperature. The discs were kept sealed in plastic throughout the test.

A servo-hydraulic Instron 1331 mechanical testing machine was used. Specimens were placed between solid loading platens and preloaded to a stress of 0.1 $MN\,m^{-2}$. This tare stress was 5% or less of the

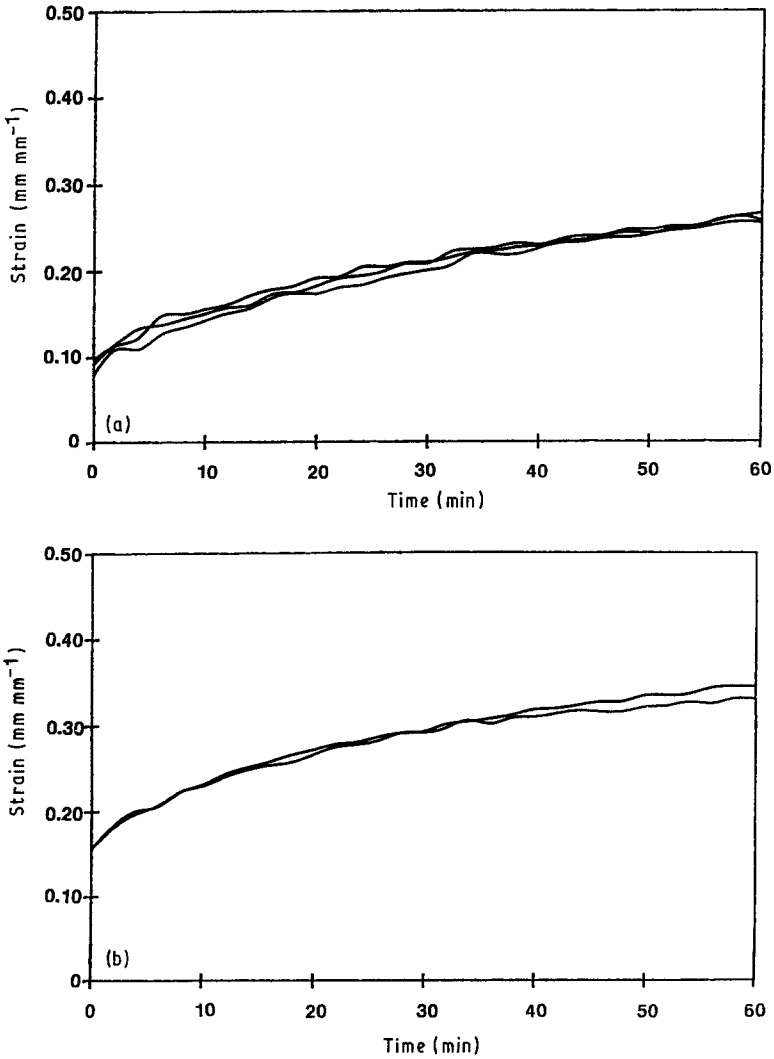

Figure 3 Creep data for all specimens tested at (a) $2\,MN\,m^{-2}$ and (b) $7\,MN\,m^{-2}$.

creep stress in any of the tests. A stress of 2, 5, 7 or $10\,MN\,m^{-2}$ was applied by driving the crosshead at a rate of $70\,kN\,sec^{-1}$ until the creep stress was achieved, then maintaining that stress for the 60 min duration of the experiment. These stress levels were chosen because they fall within the linear region of the stress–strain curve of the disc in compression [1]. Displacement against time curves were recorded and converted to strain against time by normalizing to the height of the disc measured at the periphery at rest. Two of three disc specimens loaded to $10\,MN\,m^{-2}$ failed in creep. Data from these tests were not considered in the following analysis. During the course of the test no water was seen seeping through the outer surface of the disc. However, upon removing the specimens at the conclusion of the test, a mixture of water, blood and marrow was observed on the surfaces of the loading platens.

3.2. Results and discussion

The data from creep experiments at two stress levels are shown in Figs 3a and b. Case I predicts a linear creep curve which is not observed experimentally. The experimental data do not differentiate between the models described in cases II and III. Case III is the more comprehensive model because it can account for a non-asymptotic creep curve and irreversible deformation of the disc following unloading. Data for the typical creep experiment shown in Fig. 4 are plotted according to case II (Equation 7) in Fig. 5 and according to case III (Equation 11) in Fig. 6. The osmotic pressure of the disc, P_0, as obtained from the literature, was assumed to be $0.2\,MN\,m^{-2}$ [9]. The thickness of the cartilage end-plates was determined from sagittal sections through the disc to be 0.3 mm. The system parameters K, D and G were calculated for cases II and III at four stress levels, and the results are summarized in Table I.

The contribution of the cancellous bone of the vertebral bodies to the permeability, K, was tested by increasing and decreasing the height of the bone left attached to the disc specimen. In tests using bone heights of 7 and 12.5 mm, no significant change in the parameters K, D or G was observed. This supports the hypothesis that the cartilage end-plate is the structure

TABLE I Analytical creep model parameters

	$2\,MN\,m^{-2}$ ($n = 3$)	$5\,MN\,m^{-2}$ ($n = 3$)	$7\,MN\,m^{-2}$ ($n = 2$)	$10\,MN\,m^{-2}$ ($n = 1$)
Permeability, K ($\times 10^{-17}\,m^4\,N^{-1}\,sec^{-1}$)				
Case II	0.64 (0.02)	0.33 (0.03)	0.20 (0.01)	0.21
Case III	0.85 (0.14)	0.39 (0.02)	0.27 (0.08)	0.26
Strain-dependence parameter, D ($MN\,m^{-2}$)				
Case II	10.6 (0.5)	22.8 (4.8)	37.4 (2.1)	35.5
Case III	18.2 (0.9)	34.5 (13.0)	51.1 (4.2)	52.2
Time-dependence parameter, G ($\times 10^{-6}\,MN\,m^{-2}\,sec^{-1}$)				
Case III	421 (56)	795 (360)	853 (4)	1609

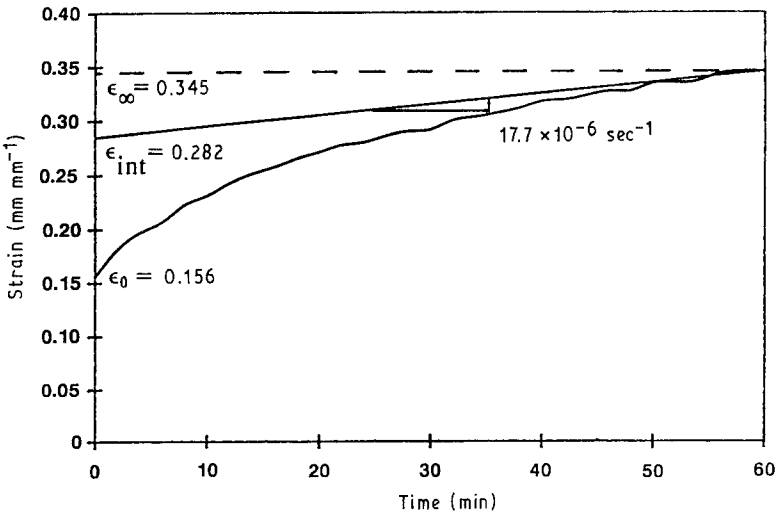

Figure 4 Creep data for a typical specimen at 7 MN m^{-2}.

that controls the flow of water from the disc during creep.

The permeability, K, was higher in case III than in case II. For the case II analysis, not all of the creep curves levelled off after 60 min, so ε_∞ was taken as the strain at 60 min, when the experiment was terminated. If the experiment had been continued for longer, a larger value of ε_∞ would probably have been found and this would have affected the value of the permeability constant obtained from the case II analysis. The permeabilities reported here are lower than the permeability of articular cartilage, reported in the literature to be in the range (2 to 8) $\times$ 10^{-17} m^4 N^{-1} sec^{-1} [5]. This is at least in part the result of the lower water content of end-plate cartilage compared with articular cartilage. End-plate cartilage was found to contain 60 to 65 wt % water as determined by freeze-drying of excised cartilage specimens. Adult articular cartilage is reported to be 85 wt % water at the superficial surface and decreases to 70 wt % at the subchondral bone [10]. It has been shown in articular cartilage that permeability decreases with decreasing water content in a non-linear manner [11, 12].

Permeability in the disc was observed to decrease with the applied stress. This is also observed in articular cartilage, where it is attributed to compaction of the cartilage matrix. This compaction results in a decrease in the size and number of pores available for water to flow through the cartilage. In the disc, it could mean that the assumption that the cartilage end-plate is incompressible may not hold at the stress levels tested or, alternatively, that the model proposed does not accommodate all of the complexities of water movement in and from the disc.

The strain-dependence parameter, D, was higher in case III than in case II, due to the introduction of the time dependence parameter, G, into the model. The value of D in case III must be greater to compensate for this additional term. Both the strain- and the time-dependence parameters increased in magnitude with stress. The variation with time of the pressure in the disc, P_d, is plotted according to case II (Equation 4) and case III (Equation 8) in Fig. 7 for two values of applied stress, 2 and 7 MN m^{-2}. The initial pressure is less than the applied stress by an amount equal to the osmotic pressure of the disc. Initially P_d decreases more rapidly for case III because the magnitude of the strain dependence, represented by the parameter D, is larger. At longer times the effect of the time-dependence parameter G causes P_d for case III to level off and the curves cross as the pressure must approach zero at long times for case II.

The relative magnitude of the strain- and time-dependent stress terms in Equation 8 for the case III analysis varies with time, since the strain-dependent term initially increases rapidly then approaches an

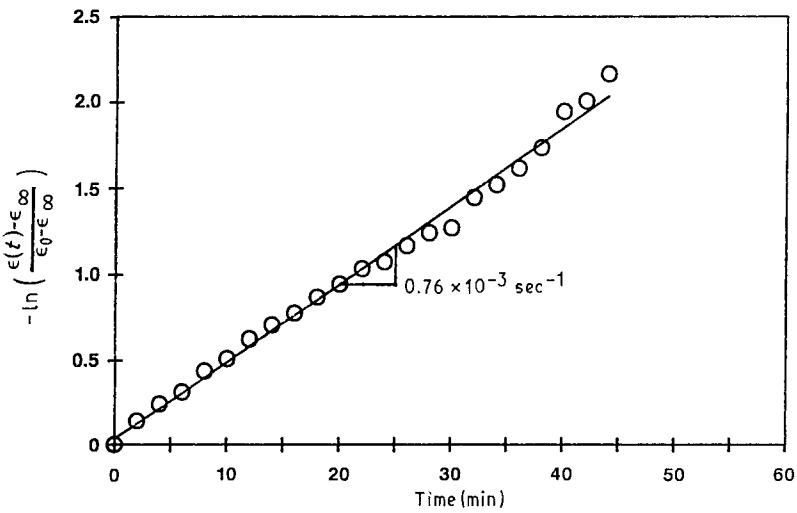

Figure 5 Creep data from Fig. 4 plotted according to case II (Equation 7).

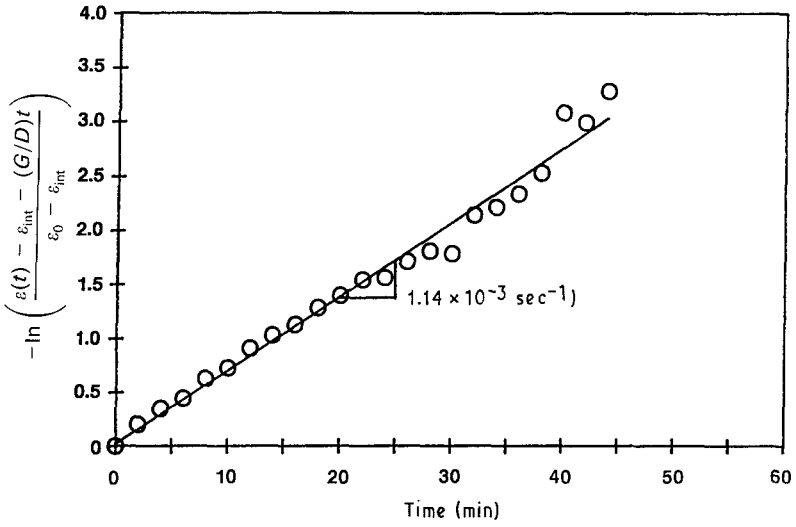

Figure 6 Creep data from Fig. 4 plotted according to case III (Equation 11).

asymptote whereas the time-dependent term increases linearly. Although the magnitude of the strain-dependence is larger throughout the duration of the experiment, its relative influence is reduced at longer times as the effect of the time-dependence parameter increases, as shown in Fig. 8.

The case II analytical model was tested with stress-relaxation data at a strain of 0.15 obtained previously on identically prepared disc specimens [1]. Values of K, D, ε_0 and ε_∞ for creep at 2, 5 and 7 MN m^{-2} were used to calculate the time at which $\varepsilon(t)$ was equal to 0.15 from Equation 7 of the case II creep model. These values of t lie on the stress-relaxation curve for a constant strain of 0.15 in Fig. 9 and thus provide confirmation that the proposed model describes the stress-relaxation response of the disc as well as the creep response. This indicates that the same mechanism is responsible for the behaviour of the disc under both loading conditions.

4. Viscoelastic models

4.1. Three-parameter model

Viscoelastic models composed of ideal elastic and viscous components are frequently used to describe a creep response such as that seen in the disc. These models cannot address physical mechanisms responsible for time-dependent behaviour in complex hierarchical systems such as the intervertebral disc. However, comparisons between these models and the analytical models of the disc do reveal the relationship between the elements of the viscoelastic models and the system parameters K, D and G.

The relationship between strain and time in the three-parameter creep model (Fig. 10a) is given by

$$\varepsilon(t) = \frac{\sigma_0}{E_1} + \frac{\sigma_0}{E_2}\left[1 - \exp\left(-\frac{t}{\tau}\right)\right] \quad (12)$$

The creep time constant is obtained from the slope when Equation 12 is plotted in the form

$$-\ln\left[\left(\frac{\sigma_0}{E_1} + \frac{\sigma_0}{E_2} - \varepsilon(t)\right)\Big/\frac{\sigma_0}{E_2}\right] = \frac{t}{\tau} \quad (13)$$

The three-parameter viscoelastic model is equivalent to the case II flow model, since upon inspection Equation 12 has the same form as Equation 5. When the terms are equated, the modulus, E_2, is related to the strain-dependence parameter D by

$$E_2 = D\sigma_0/(\sigma_0 - P_0) \quad (14)$$

Equating the exponential terms in Equations 5 and 12, the creep time constant is related to both the permeability, K, and the strain-dependence parameter, D:

$$\tau = h_i L/2KD \quad (15)$$

4.2. Four-parameter model

The relationship between strain and time in the four-parameter creep model (Fig. 10b) is given by

$$\varepsilon(t) = \frac{\sigma_0}{E_1} + \frac{\sigma_0}{E_2}\left[1 - \exp\left(-\frac{t}{\tau}\right)\right] + \frac{\sigma_0}{\eta_1}t \quad (16)$$

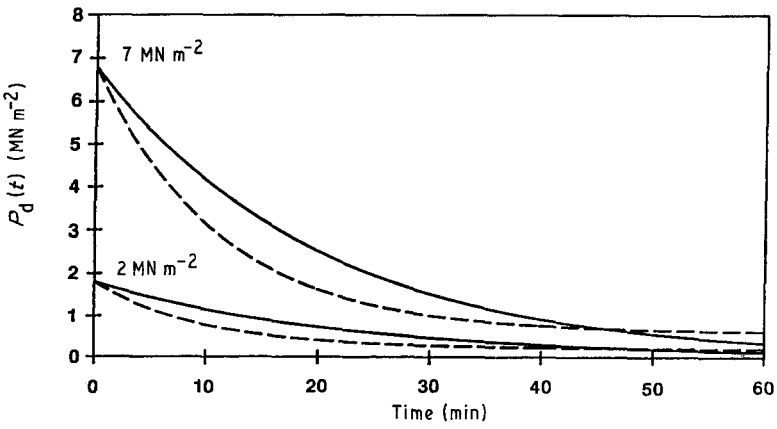

Figure 7 Pressure in the disc as a function of time for (——) case II and (– – –) case III.

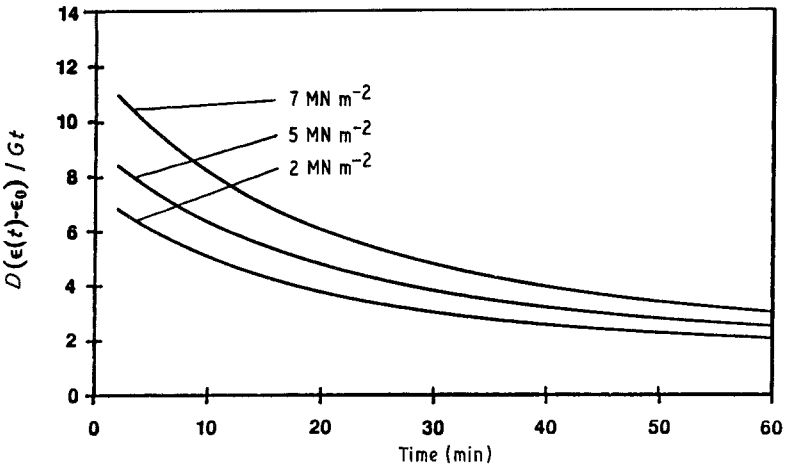

Figure 8 Ratio of the magnitudes of the strain- and time-dependence terms for case III as a function of time.

At long times the exponential term in Equation 16 becomes negligible and the creep curve is linear:

$$\varepsilon(t) = \frac{\sigma_0}{E_1} + \frac{\sigma_0}{E_2} + \frac{\sigma_0}{\eta_1} t \quad (17)$$

Since $\sigma_0/E_1 = \varepsilon_0$, the intercept of the linear, long-time region of the creep curve with the strain axis is $\sigma_0/E_2 + \varepsilon_0$ and the slope is σ_0/η_1.

The creep time constant is obtained by plotting Equation 16 in the form

$$-\ln\left[\left(\frac{\sigma_0}{E_1} + \frac{\sigma_0}{E_2} + \frac{\sigma_0}{\eta_1} t - \varepsilon(t)\right) \Big/ \frac{\sigma_0}{E_2}\right] = \frac{t}{\tau} \quad (18)$$

Comparison of Equations 16 and 9 reveals that the four-paramenter viscoelastic model is equivalent to the case III flow model. By equating terms, the modulus, E_2, of the four-parameter model is related to the strain-dependence parameter D and the time-dependence parameter G by

$$E_2 = \frac{2KD^2\sigma_0}{2KD(\sigma_0 - P_0) - h_i LG} \quad (19)$$

Equating the exponential terms of Equations 9 and 16, the time constant τ is related to both the permeability K and the strain-dependence parameter D:

$$\tau = h_i L/2KD \quad (20)$$

The viscosity, η_1, which represents the non-recoverable strain, is related to the strain- and time-dependence parameters by

$$\eta_1 = \sigma_0 D/G \quad (21)$$

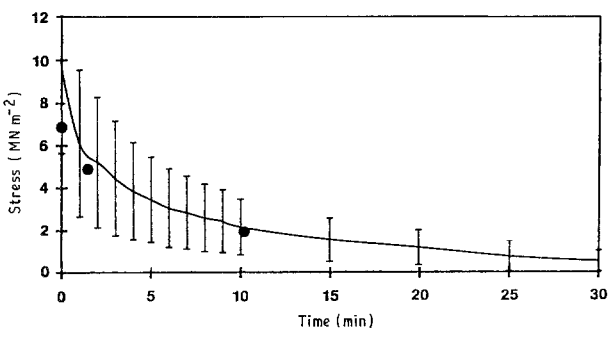

Figure 9 Stress relaxation data for a compressive strain of 0.15 from [1] and calculated points from the creep model assuming case II behaviour.

4.3. Results and discussion

Values for the elements of the three- and four-parameter models were calculated from experimental data using plots of the form given by Equations 13 and 18 and are summarized in Table II. The time constant τ is independent of the applied stress in both the three- and the four-parameter models, which means from Equations 15 and 20 that the product KD is a constant for both cases II and III. The viscoelastic parameters E_1, E_2 and η_1 all increase with applied stress with the possible exception of η_1 from the single 10 MN m^{-2} test. Comparison of a typical creep experiment with the calculated curves for the three-parameter model (Equation 12) and the four-parameter model (Equation 16) shows that both models fit the data (Fig. 11). The four-parameter model is more attractive because it can accommodate an irreversible component of deformation.

Kaleps and co-workers fitted a three-parameter viscoelastic model to experimental creep data from intervertebral discs harvested from rhesus monkeys and humans [13, 14]. They employed an interpolation and optimization scheme to obtain values for E_1, E_2 and η_1. All of the human discs were loaded at stress levels well below those employed in this study (0.1 to 0.4 MN m^{-2}). However, a limited number of monkey specimens were loaded at levels of 2 MN m^{-2}, and these results are compared in Table III. The creep curve calculated with their values for a three-parameter model has a much higher initial strain and is a flatter creep curve. These differences probably result from

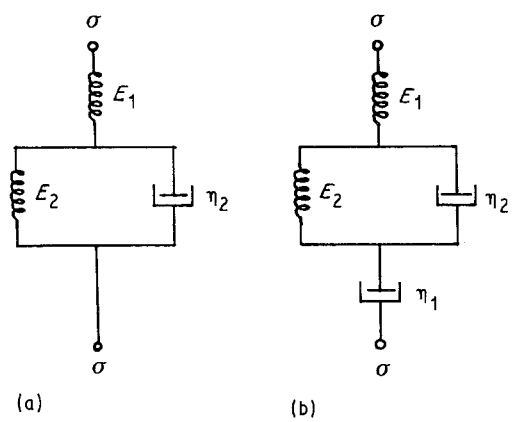

Figure 10 Viscoelastic solid models: (a) three-parameter model and (b) four-parameter model.

TABLE II Viscoelastic model parameters

	$2\,MN\,m^{-2}$ ($n = 3$)	$5\,MN\,m^{-2}$ ($n = 3$)	$7\,MN\,m^{-2}$ ($n = 2$)	$10\,MN\,m^{-2}$ ($n = 1$)
Three-parameter model elements				
τ (sec)	1416 (88)	1342 (94)	1224 (133)	1297
E_1 ($MN\,m^{-2}$)	22.4 (2.5)	37.5 (4.4)	44.9 (0.1)	63.3
E_2 ($MN\,m^{-2}$)	11.8 (0.6)	23.8 (5.0)	38.6 (2.2)	36.2
Four-parameter model elements				
τ (sec)	544 (191)	811 (268)	703 (246)	719
E_1 ($MN\,m^{-2}$)	22.4 (2.5)	37.5 (4.4)	44.9 (0.1)	63.3
E_2 ($MN\,m^{-2}$)	23.7 (1.2)	41.0 (15.8)	57.6 (2.8)	60.5
η_1 ($\times 10^3\,MN\,sec\,m^{-2}$)	78.5 (18.6)	226 (39)	419 (33)	324

TABLE III Comparison of viscoelastic model parameters for $\sigma_0 = 2\,MN\,m^{-2}$

	Present work	[13, 14]
τ (sec)	1416 (88)	4812 (1761)
E_1 ($MN\,m^{-2}$)	22.4 (2.5)	9.7 (4.7)
E_2 ($MN\,m^{-2}$)	11.8 (0.6)	8.7 (2.5)

species differences as well as from specimen preparation and test conditions. In their work discs were deep frozen before testing, and the posterior articulations were left intact during the test. It is known that freezing the disc before testing causes ice crystals to form in the disc structure, which can disrupt the collagen architecture of the disc and alter the water content [15]. The presence of intact articulating facets would alter the configuration of the compressive load, particularly at higher strain, from a uniaxial compression to a combination of compression and shear stresses. The effect of varying the applied compressive stress on the values for elements in the viscoelastic model is also addressed in the Kaleps data. Although the variability in results between discs at similar stress levels is high, the trends observed are similar to those in this study. Specifically, the moduli increase with increasing applied stress, whereas the time constant appears to remain essentially constant.

5. Conclusions

Models for the compressive creep response of intervertebral disc have been developed. These are based on previous observations that the time-dependent mechanical response arises from the transport of water out of the disc through the cartilage end-plates into the vertebrae. Assuming that the driving force for water transport is a pressure gradient across the cartilage between the disc and the vertebral bodies caused by an external stress, the following conclusions can be drawn.

1. The experimental creep data fit models which consider the strain-dependence or strain- and time-dependence of the pressure in the disc. System parameters obtained from analysis of creep data also correctly predict the stress relaxation.

2. These models are analogous to the three- and four-parameter viscoelastic models, but contain elements directly relatable to the physical structure.

3. The permeability of the end-plate cartilage calculated from these models is slightly lower than that reported for articular cartilage; differences in the water content of the cartilages may account for this.

Acknowledgement

This research was generously supported by the Army Research Office, grant number DAAL03-88K-0097.

References

1. J. J. CASSIDY, A. HILTNER and E. BAER, *J. Mater. Sci.: Mater. Med.* **1** (1990) 69.
2. V. C. MOW *et al.*, *J. Biomech. Eng.* **102** (1980) 73.
3. W. C. HAYES and L. F. MOCKROS, *J. Appl. Physiol.* **31** (1971) 562.
4. G. E. KEMPSON, in "Adult Articular Cartilage" (Pitman Medical, Kent, 1979) p. 333.
5. V. C. MOW, M. H. HOLMES and W. M. LAI, *J. Biomech.* **17** (1984) 377.
6. R. Y. HORI and L. F. MOCKROS, *ibid.* **9** (1976) 259.

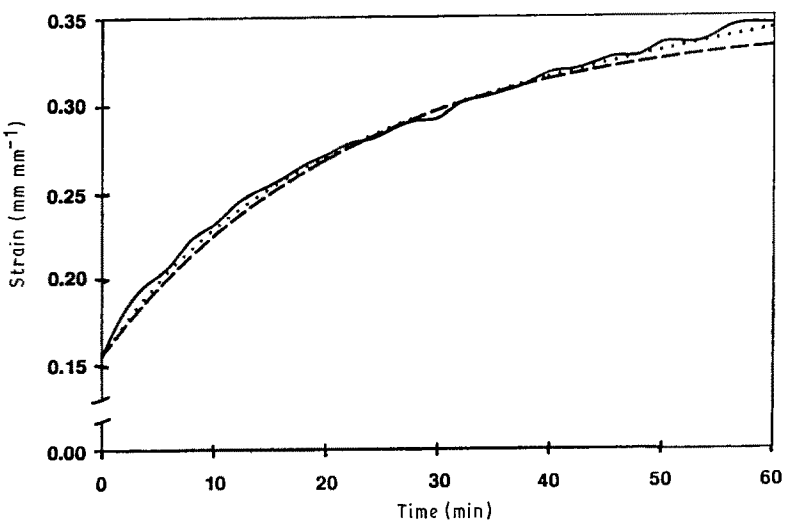

Figure 11 Creep data for a typical specimen (——) compared with (– – –) the three-parameter model (Equation 12) and (· · ·) the four-parameter model (Equation 16).

7. J. J. CASSIDY, A. HILTNER and E. BAER, *Connect. Tissue Res.* **23** (1989) 75.
8. J. KASTELIC and E. BAER, in "The Mechanical Properties of Biological Materials" (Society of Experimental Biology, London, 1980) p. 397.
9. R. C. QUINNEL, H. R. STOCKDALE and D. S. WILLIS, *Spine* **8** (1983) 166.
10. H. LIPSHITZ, R. ETHERIDGE and M. J. GLIMCHER, *J. Bone. Joint Surg.* **A58** (1976) 1149.
11. C. G. ARMSTRONG and V. C. MOW, *ibid.* **A64** (1982) 88.
12. A. MAROUDAS, *Biorheology* **12** (1975) 233.
13. I. KALEPS, L. E. KAZARIAN and M. L. BURNS, *J. Biomech.* **17** (1984) 131.
14. M. L. BURNS, I. KALEPS and L. E. KAZARIAN, *ibid.* **17** (1984) 113.
15. J. O. GALANTE, *Acta Orthop. Scand. Suppl.* **100** (1967) 1.

Received 8 December 1989
and accepted 10 January 1990